

# Bioinspired four-dimensional polymeric aerogel with programmable temporal-spatial multiscale structure and functionality

Wenxin Wang<sup>a,\*</sup>, Liwen Du<sup>a</sup>, Yu Xie<sup>b</sup>, Fenghua Zhang<sup>c</sup>, Peng Li<sup>d</sup>, Fang Xie<sup>e</sup>, Xue Wan<sup>c</sup>, Qibing Pei<sup>b</sup>, Jinsong Leng<sup>c,\*\*</sup>, Ning Wang<sup>a,\*\*\*</sup>

<sup>a</sup> State Key Laboratory of Marine Resource Utilization in South China Sea, Hainan University, Haikou, 570228, China

<sup>b</sup> Department of Materials Science and Engineering, Henry Samueli School of Engineering and Applied Science, University of California, Los Angeles, CA, 90095, USA

<sup>c</sup> Center for Composite Materials and Structures, Harbin Institute of Technology, Harbin, 150080, China

<sup>d</sup> College of Physical Science and Technology, Heilongjiang University, Harbin, 150080, China

<sup>e</sup> School of Naval Architecture and Ocean Engineering, Harbin Institute of Technology at Weihai, Weihai, 264209, China

## ARTICLE INFO

### Keywords:

Shape memory polymer  
Programmable  
Fixable temporary shape  
Stimuli-responsive  
Temporal-spatial multiscale

## ABSTRACT

The original four-dimensional (4D) polymeric aerogel design introduces a concept of programmable temporal-spatial multiscale structure, in which the fourth dimension is time. The novel aerogel possesses shape memory properties, which can fix temporary state and recover permanent state by releasing frozen stress under stimulus without any sophisticated electro-mechanical equipment in the programmable manner. Its structure can be tailored by precrosslinked ice template method to obtain high permeable multiscale structure. Its functionalities and performances can be customized and optimized by adjusting porous framework, matrix, functional groups, and self-adaptivity based on application demands. Comparing with traditional aerogels, the emerging 4D aerogel has many unique properties, including excellent self-adaptivity, high permeable multiscale structure, flexible preprogrammed ability, customized functional groups, low cost, and environmental friendliness. Its exploration and development could draw much attention due to various promising potential applications including water treatment, intelligent structure, and sensor. These high-value applications would further promote the development of the intelligent aerogels and the reliable preparation technologies. As an interesting field, the 4D aerogel idea is revolutionary for traditional aerogels and expected to provide new perspective and practical approach to realize the integration of material, structure, and functionality.

## 1. Introduction

There are many challenges in designing, preparing, and engineering intelligent material and structure. The intelligent material is one of the most popular research fields in materials science. Design, construction, and intelligence of porous materials have long been an essential subject. There are visible differences between the structure-controllable design and synthesis of macroporous, mesoporous, and microporous materials. Generally, the network framework of macroporous/mesoporous materials usually lacks large specific surface area. The microporous materials have ultrahigh specific surface area but often lack rational mass transfer pathways [1]. Therefore, the development of hierarchical porous materials that simultaneously possesses suitable macroporous, mesoporous,

and microporous is very desirable.

As one of the most distinctive and useful porous materials, the aerogels have attracted considerable interest owing to their high permeable, self-similar, and tailored fractal structure of random or statistical significance [2–4]. The aerogel derives from the gel, in which liquid component of the gel replaced by gas. Its porous frameworks can be customized based on specific applications, accumulated knowledge, and rational design. It has wide applied prospects such as water purification, aerospace, sensors, electromagnetic shielding, catalysts, super capacitor, and armor [5–8]. Recently, the polymeric aerogels are developing promptly due to their unique characteristics, including easily customized porous frameworks and functionalities [9]. The common polymeric aerogels are obtained from alginate, chitosan, polyurethane,

\* Corresponding author.

\*\* Corresponding author.

\*\*\* Corresponding author.

E-mail addresses: [wangwenxin.999@163.com](mailto:wangwenxin.999@163.com) (W. Wang), [lengjs@hit.edu.cn](mailto:lengjs@hit.edu.cn) (J. Leng), [wangn02@foxmail.com](mailto:wangn02@foxmail.com) (N. Wang).

polystyrene, polyimide, polyurea, poly ( $\alpha$ -lactid acid), and poly (vinylidene fluoride) [9,10]. However, it is noteworthy that the intellectualization of the aerogel also remains a great challenge.

As a remarkable intelligent material, shape memory material can transform from a temporary “freezing” state to a permanent state induced by right stimulus. Recently there is report about deformable cellulose nanocrystal-based aerogels without the ability of programmable and fixable temporary shape [5], whereas the temporary shape of the shape memory material can be always maintained unless the right stimulus triggers its shape recovery. Although some graphene aerogel composites have good electro-thermal-induced shape memory effect [3, 6], their single stimulus mode, complex synthetic process, and high cost in raw material have become the bottleneck of them extensive application. Those works on shape memory aerogel focused on a single deformable purpose or electro-thermal-induced composites rather than simple and flexible polymeric intelligent aerogels. The new strategies are still highly desired. So far, however, the self-adaptive polymeric aerogel, which merges advantages of porous materials and shape memory polymers, has not yet been reported.

It is inspiring to see there are multifarious attractive hierarchical structures in nature, such as porifera, coral, honeycomb, cork, alveoli, and pomelo peel [1,11]. This work develops an original self-adaptive polymeric aerogel with the capacity of fixable temporary state, programmable temporal-spatial multiscale structure and multi-stimuli responsive performance, taking inspiration from them. The excellence of the novel aerogel is attributed to the following points. First, this aerogel with a high permeable three-dimensional (3D) multiscale structure can be designed to suit various applying requirements. Then, it has good processibility and functionalization, which are important advantages in practical applications. Moreover, the multiformity of its synthetic route benefits to incorporate multifunctionality with its multiscale spongy framework. Finally, and the most importantly, the 3D multiscale structure of the functionalized aerogel can be programmed under environmental stimulation over time, which is generally unavailable in other types of traditional aerogels like silica aerogel, carbon aerogel, or metal oxide aerogel. In general, crystalline domains, stiff chains, physical cross-linked points, and chemical cross-linked points of the molecular network are responsible for the permanent state of shape memory polymers. Meanwhile, melting/crystalline or rubber/glass transitions of these materials usually act as switches to change the structure of the molecular network. The above key points provide abilities of programmable time evolution and energy absorption to shape memory polymers [12–18]. In a 4D space, an object lasts through time, just like it extends through space [19]. An object that exists in time has temporal parts [19–22]. The temporary intrinsics involve properties of an object, which are intrinsic and temporary [20]. Shape is regarded as one of the temporary intrinsics. If an object has a particular shape and also changes its shape over time, there must be some particular ability. Shape memory material has the ability for fixing temporary state and responding to environmental stimulation in the programmable manner. It can change its state, including volume or configuration, in response to stimuli such as heat, chemical, light, electricity, microwave, and magnetic field [15,23]. Based on the ability to change state with time in the programmable manner, these shape memory materials with 3D structure also can be regarded as 4D material in which the fourth dimension is time [24–31].

In order to distinguish the intelligent aerogels from other traditional aerogels, the aerogels with the ability to transform state over time in the programmable manner can be defined as 4D aerogel. In this work, the fourth dimension of poly (vinyl alcohol) (PVA) based 4D aerogel stems from programmable shape memory characteristic with time evolution. The 4D aerogel has three significant advantages in combination with the results of this work and relevant literatures.

First, unlike almost all other traditional aerogels, the 4D aerogel possesses programmable fixable and multi-stimuli responsive capacity. Its water-induced and thermal-induced shape memory effects are shown

in Fig. 1a. It can fix programmable temporary state and recover permanent state induced by controlled main influence factors. Herein, the plasticizing effect of water triggers its shape memory behavior with increasing flexibility of its macromolecule chains [32–34]. Moreover, the 4D aerogel also has a remarkable thermal-induced shape memory effect without water. Its cross-linked molecular network mainly controls its self-adaptive ability. That means the fourth dimension of the 4D aerogel results from programmable time evolution via designs of material composition, structure, and process parameters. There are clearly different from conventional aerogels and discussed in detail later in this article.

Second, the 4D aerogel is constructed via a precrosslinked ice template strategy that could easily control microstructure, apply to many shapes, and produce various materials. As shown in Fig. 1b, typical PVA-based 4D aerogel is obtained from the precursor system of PVA, glutaraldehyde (GA), and deionized water. Firstly, the PVA solution is mixed with GA, forming a precursor. Then the precursor forms precrosslinked network at the acidic condition. Herein, the GA works as cross-linker in the precursor system. The carbonyl groups of GA and abundant hydroxyl groups on the PVA molecular chain can play a key role in the crosslinked network. When the precrosslinked precursor system is frozen at  $-60\text{ }^{\circ}\text{C}$ , there are two micro-phase including the concentrated precrosslinked matrix and ice crystal phase in the frozen system. It is well documented in the literature that the molecular chains of polymer network in the concentrated precrosslinked matrix can be stressed by the internal force during ice crystal formation [35]. The ice crystal phase is removed with sublimation for forming the multiscale spongy framework, as shown in Fig. 1b. Since the morphology and sublimation of ice crystals influence the morphology of spongy framework, the multiscale microstructure of the 4D aerogel can be tuned by manipulation of the lyophilization conditions such as the freezing temperature and time. The 4D aerogel with programmable multiscale structure is ultimately gained after lyophilization and post-curing treatment with gelation and formation of complete crosslinked network [36]. The scanning electron microscope (SEM) images of the 4D aerogel with different precrosslinked time show that the spongy framework can be tuned by precrosslinked time, in Fig. 1b. Later in this article, the influences of GA content and post-curing for multiscale spongy framework are discussed in detail. The viscosity increase of precursor at the acidic condition and slight shrink after post-curing also suggest that the precrosslinked precursor system has some crosslinked polymer molecular chains forming partial polymer network. Except polymer network, other linear PVA molecular chain and GA in the precrosslinked precursor system can crosslink while lyophilization, forming relaxed polymer molecular chain segments and leading to permanent spongy framework [35]. In the precrosslinked precursor system, the crosslinked network part and other polymer molecules part both are important for controlling the microstructure of the 4D aerogel. This precrosslinked method can achieve a controllable 3D multiscale structure in the micro-nano scale. Furthermore, the thermal transition of the PVA-based matrix also is crucial for this programmable 4D aerogel with the multiscale spongy framework [36,37]. Therefore, its programmable multiscale spongy framework can be tuned by material, precrosslinked, lyophilization, and post-curing parameters.

Third, the 4D aerogel can adjust 3D multiscale structure and chemical components to meet various practical requirements, which means it has many potential applications. The absorption capability of PVA-based 4D aerogel and melamine sponge is compared in the initial concentration of crystal violet solution (Fig. S1 and Movie S1). The results reveal their conspicuous dissimilarity of absorption capability at once. In the first adsorption process, the 4D aerogel immediately absorbed all the crystal violet solution, but melamine sponge only absorbed a part of the crystal violet solution. The second and third adsorption processes are simulated pulsion-suction cycle experiments. The dissimilarity is remarkably clear via comparison of initial crystal violet solution, residual liquids, squeezed liquids, and samples. Interestingly enough, the

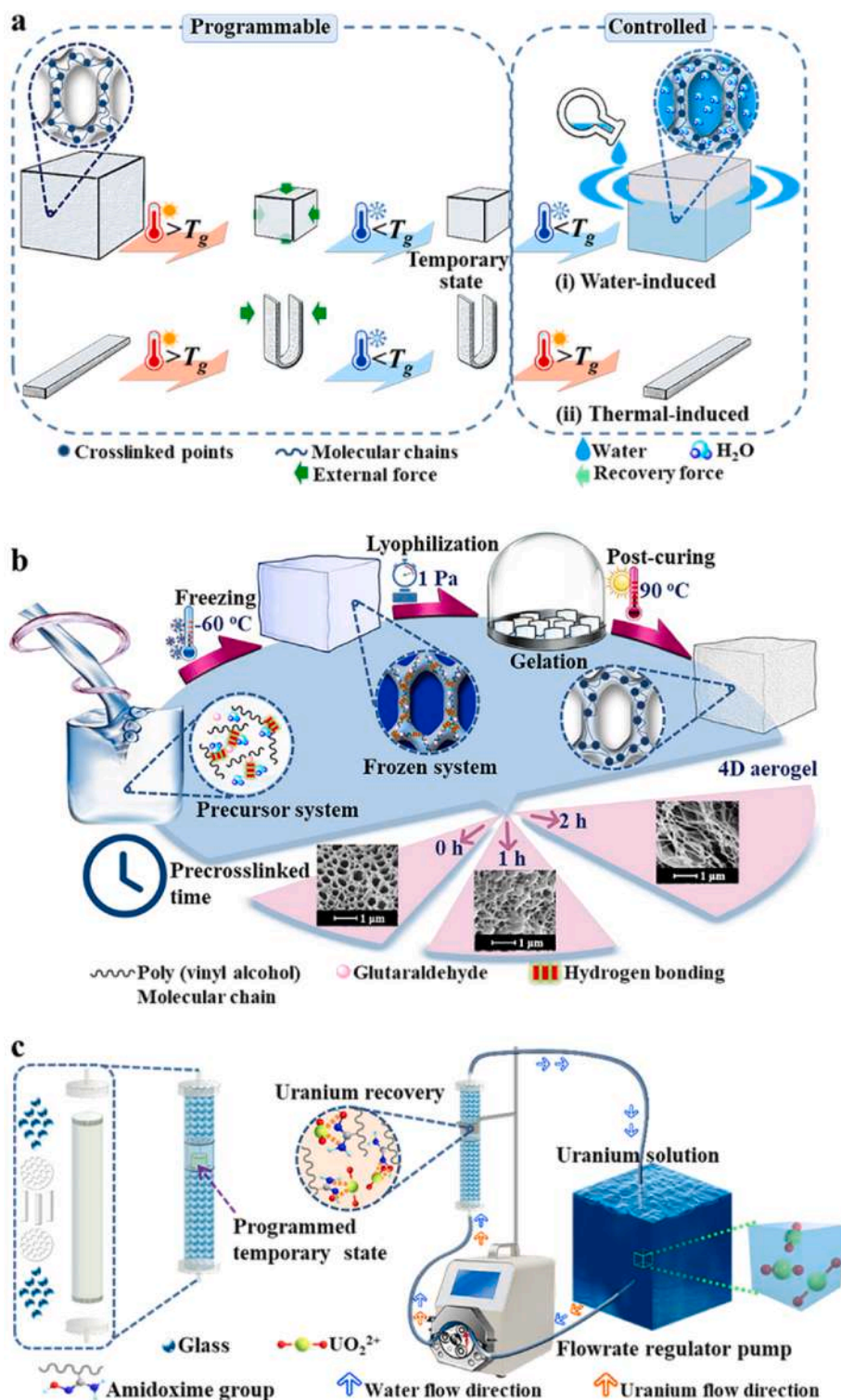


**Fig. 1.** Structure and functionality design strategies of programmable 4D aerogel. (a) The fourth dimension of this 4D aerogel stems from shape memory characteristic with time evolution. Its programmable multi-stimuli responsive processes include fixing and recovering. (b) Constructed process of programmable 4D aerogel with a multiscale spongy framework. (c) Flow-through adsorption performance test system for the pulsion-suction cycle adsorption experiment of functionalized 4D aerogels.

4D aerogel absorbed all crystal violet over and over again, however, melamine sponge no more adsorption occurred. After the extrusion process, crystal violet is still firmly absorbed in the 4D aerogel, but it is removed with water from melamine sponge. Meanwhile, the 4D aerogel remained dark purple with all absorbed crystal violet, and melamine sponge changed from dark purple to lavender with expelling some crystal violet solution. These results suggest that the 4D aerogel has excellent cycle adsorption and enrichment ability. This work built a flow-through adsorption performance test system for the pulsion-suction

cycle adsorption experiment of the functionalized 4D aerogel based on the above results and previous work (Fig. 1c). The self-adaptivity, multiscale spongy framework, and functional groups are critical elements for adsorption efficiency and potential of the programmable 4D aerogel.

Supplementary data related to this article can be found at <https://doi.org/10.1016/j.compscitech.2021.108677>.

## 2. Results and discussion

### 2.1. Chemical properties and controllable microstructure

As expected, chemical property and multiscale spongy framework of the 4D aerogel is programmed by cross-linker content and precrosslinked parameters (Fig. 2). The precrosslinked ice template strategy is schematically illustrated in Fig. 1b for constructing the 4D aerogel. The PVA-based 4D aerogel is designated as x-GA-PVA, in which GA is x volume percent of the precursor system. There are 1-GA-PVA, 2-GA-PVA, 3-GA-PVA, 4-GA-PVA, and 5-GA-PVA, respectively. For comparison, pure PVA without GA is designated as PVA. X-ray powder diffraction (XRD), Fourier transform infrared (FTIR) spectra, and X-ray photoelectron spectroscopy (XPS) indicate that there are covalent bonding and/or hydrogen bonding between PVA and GA, as shown in Fig. 2 and Fig. S2. It is well known that PVA is a typical semicrystalline polymer due to the strong hydrogen bonding between abundant hydroxyl groups [36]. As shown in Fig. 2a, the introduction of GA disturbs the hydrogen bonding of PVA molecular chain as well as its crystal structure, leading to decrease its crystallinity. The shape memory fixity is mainly attribute to the crosslinking between hydroxyl groups and carbonyl groups in the amorphous polymer chains [35]. Therefore, the amorphous polymer structure plays a key role in shape memory process. The characteristic groups of the PVA-based 4D aerogel are confirmed from FTIR and XPS spectra (Fig. 2b and c). This 4D aerogel consists of a cross-linked PVA matrix. The higher GA content brings about greater cross-linked ability within a certain range. The cross-linked polymer chain of 4D aerogel is helpful for its deformation in the shape memory process [32].

SEM images show that 4D aerogels have a high permeable 3D multiscale spongy framework. In Fig. 2 and Fig. S3, the morphology of its

porous architecture changes with the precrosslinked time and the cross-linker content. As the increase of GA content, the 4D aerogel has a smaller average pore size, narrower pore size distribution, and closer pore arrangement, accompanying higher crosslink density. It can be speculated that the nanofibrous structure of the 4D aerogel also may vary considerably with crosslink density. Herein, the programmable multiscale spongy framework of 5-GA-PVA is further optimized by precrosslinked parameters. As illustrated in Fig. 2 and Fig. S4, the average diameter of nanofibrous structure is about 100 nm with uniform morphology and homogeneous distribution. The quantity of nanofibrous structure grows along with precrosslinked time. However, its porous frameworks get even more incompact and irregular. These structural characterizations of the 4D aerogels indicate that cross-linker content and precrosslinked parameters have critical effects on size, morphology, distribution, and quantity of micro-nano aperture and nanofibrous structure. Moreover, this interconnected 3D network structure provides channels for liquid spreading. Thus, there is a benefit for chemical interaction and physical absorption between the 4D aerogel and the solutions.

### 2.2. Thermodynamic properties

The thermodynamic analysis measurement including thermal gravimetric analysis (TGA), differential scanning calorimeter (DSC), and dynamic mechanical analysis (DMA) are carried out to further prove the effect of GA content and post-curing on the PVA-based 4D aerogel structure. The thermal stability of all samples is compared, including thermal degradation and carbonization degradation. As illustrated in Fig. S5, the 4D aerogel contains little water, which is mainly attributed to water binding capacity of free hydroxyl groups [38]. It quickly dehydrates at about 50 °C, because of the interaction between water and

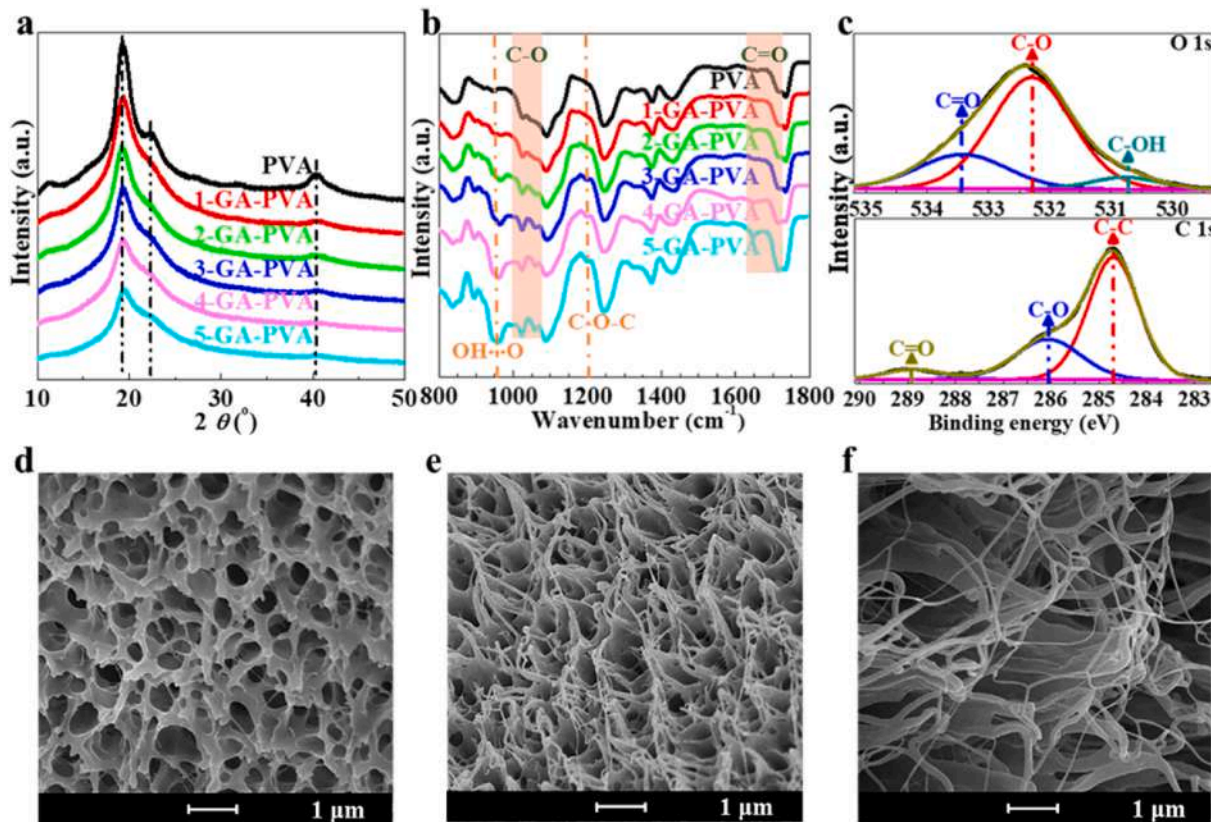


Fig. 2. Chemical property and controllable microstructure. (a) XRD pattern and (b) FTIR spectra of PVA and x-GA-PVA with different GA content: 1-GA-PVA, 2-GA-PVA, 3-GA-PVA, 4-GA-PVA, 5-GA-PVA. (c) High-resolution XPS spectra of the O1s and the C1s regions for 5-GA-PVA. (d–f) SEM images of 5-GA-PVA with different precrosslinked time: (d) 30 min, (e) 60 min, (f) 90 min, respectively.

hydroxyl groups is weakened with rising temperature. Then the micro-molecules detach from lateral groups of polymer chains within about 230 °C. It starts to decompose above approximately 230 °C, as evidenced by the rapid decrease in weight, and only little organic components remain.

As can be seen from Fig. 3a and Fig. 3b, the 4D aerogel still keeps excellent thermal stability and high permeable spongy framework after post-curing treatment. At the same time, thermal weightlessness of the 4D aerogel has decreased significantly within 100 °C, while crystal peaks of XRD and infrared characteristic peaks have noticeable changes (Fig. S6). All the endothermic and exothermic peaks of DSC thermogram shift to slightly higher temperature with an increase of GA content (Fig. 3c and Fig. S7), though the addition of small amount GA in the PVA-based 4D aerogel has no significant effect on its thermal transitions. As can be seen from Fig. 3c, its glass transition temperature ( $T_g$ ) slightly increases with the GA content as well, in combination with DMA thermogram and previous work [36]. It suggests that its  $T_g$  can be adjusted by GA content. The  $T_g$  of cross-linked 5-GA-PVA is about 85 °C. Here, its chain segment mobility is conditioned with the increase of crosslink density. The external energy is able to be stored effectively in the 3D multiscale spongy framework of the 4D aerogel below  $T_g$  and entirely released above  $T_g$ . These results show that the introduction of GA has a significant effect on the crosslink density of the 4D aerogel, and disturbs its hydrogen bonding influencing its crystallization. There are also evident in XRD, FTIR, and XPS results.

### 2.3. Multi-stimuli responsive capacity

To substantiate the multi-stimuli responsive effect of the 4D aerogel, water-induced and thermal-induced shape memory behaviors are characterized, respectively (Fig. 4). An example of deployable 4D aerogel is demonstrated in Fig. 4a and Movie S2, which is able to recover permanent state at about 4 s in water. This is much faster than the most previous water-induced shape memory polymers in the literature

(Table S1).

Supplementary data related to this article can be found at <https://doi.org/10.1016/j.compscitech.2021.108677>.

Generally, traditional water-induced shape memory polymers without microstructure require hours to finish the stimuli-responsive process. In contrast to these traditional water-induced shape memory polymers, the 4D aerogel has a higher water-induced recovering ratio and shorter water-induced recovery time. Besides, the 4D aerogel also shows better water-induced stimuli-responsive performance than hydrophobic porous shape memory material and drying natural cellular material.

As shown in Fig. S8, water-induced stimuli-responsive speed of the 4D aerogel is tuned by temperature and its thickness. In accordance with Figs. 2 and 3, it can be inferred that excellent water-induced stimuli-responsive capacity of the 4D aerogel is mainly attributed to its high permeable multiscale spongy framework and chemical property. In order to further verify these active influence factors, the contact angle tests of representative PVA-based 4D aerogel and PVA are carried out (Fig. S9 and Movie S3). There are also the control groups that are prepared under the same conditions without precrosslinked and lyophilization processes for comparison purposes. The contact angles of 5-GA-PVA and PVA with the spongy framework are about 0°. The water drops quickly spread over and permeate after contacting with PVA-based aerogel, but there are different for the samples without pore. The contact angles of 5-GA-PVA and PVA without microstructure are  $50.2^\circ \pm 0.1^\circ$  and  $65.2^\circ \pm 0.1^\circ$ , respectively. As illustrated in Fig. 2 and Fig. S9, cross-linked samples have larger polar groups, so their contact angles are smaller. The super hydrophilicity of PVA-based 4D aerogel is related to its high permeable multiscale structure and numerous polar groups, which also are benefits to imbibe solution and reach diffusive equilibrium quickly. And the hydrogen bond can be easily weakened by water [5]. The results of the swelling behavior test also confirm that crosslink density, multiscale spongy framework, and polar groups of the 4D aerogel are critical for diffusion speed and permeability (Fig. S10).

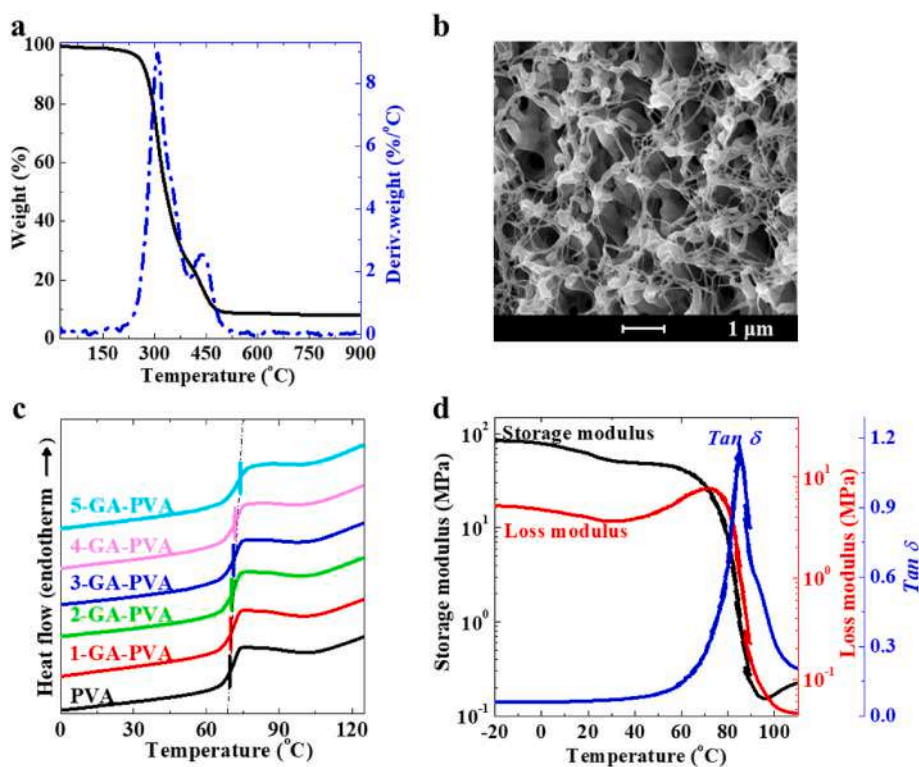
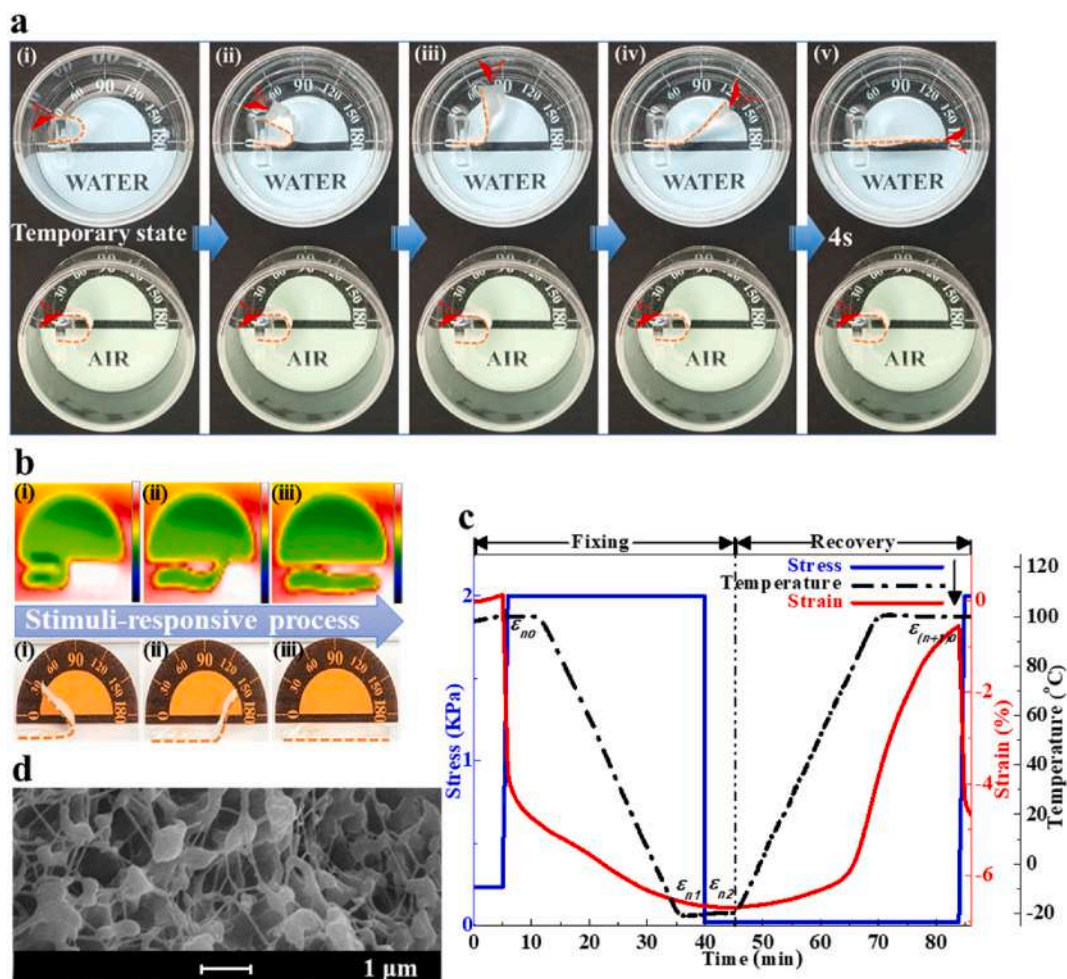


Fig. 3. Thermodynamic properties. (a) TGA analysis and (b) SEM image of 5-GA-PVA after post-curing treatment. (c) DSC curves (second heating) of PVA and x-GA-PVA with different GA content: 1-GA-PVA, 2-GA-PVA, 3-GA-PVA, 4-GA-PVA, 5-GA-PVA. Curves have shifted vertically to allow for comparison. (d) DMA thermogram of 5-GA-PVA.



**Fig. 4.** Multi-stimuli responsive performance. (a) Water-induced shape memory process at room temperature. In each photo: the top one is PVA-based 4D aerogel in water, and the under one is PVA-based 4D aerogel in the air for comparison. (b) Thermal-induced shape memory process of PVA-based 4D aerogel. Top: infrared thermal images. Under: photos. (c) Thermodynamic compression experiment of PVA-based 4D aerogel. (d) SEM image of PVA-based 4D aerogel after the deformation-recovery cycle.

The diffusion speed is one of the most critical factors for determining water-induced stimuli-responsive recovery efficiency and chemical or physical interaction efficiency between solute and the 4D aerogel in solution before the equilibrium [32]. The results of water-induced shape memory behavior, hydrophilic property, swelling behavior, and absorption capacity tests suggest that high permeable multiscale structure, larger polar groups, crosslink density, thickness, and temperature are basic conditions for programming water-induced shape memory performance of the 4D aerogel (Table S2).

Supplementary data related to this article can be found at <https://doi.org/10.1016/j.compscitech.2021.108677>.

Additionally, the 4D aerogel rapidly recovered to its original state under heat control (Fig. 4b and Movie S4). The temperature dependence of the dynamic compression tests of PVA-based 4D aerogel is shown in Fig. 4c. The black curve represents the temperature, the red curve represents the strain, and the blue curve represents the stress. The test parameters of its fixing and recovery program are detailed in the experimental materials and methods part (Supporting Information). The  $\epsilon_{n2}$  is the ultimate strain with the stress-free state in fixing process. The  $\epsilon_{n1}$  is the strain under a constant stress in fixing process and the  $\epsilon_{(n+1)0}$  is the final strains with the stress-free state in recovery process and the  $\epsilon_{n0}$  is the initial strains with the stress-free state during the continuous fixation and recovery cycles. Its fixing ratio ( $R_f$ ) and recovering ratio ( $R_r$ ) are above 90% in the second cycle, calculating via equations 4 and equations 5 in the Supporting Information. Its programmable and

reversible transitions between permanent and temporary states are demonstrated by cyclic thermodynamic compression experiments, as shown in Fig. S11. The  $R_f$  and  $R_r$  are maintained at about 95% during three repeated programming cycles in the appropriate lab environment without limited by instruments parameter and with higher strain rate. Such a fixing and recovery cycles can be repeated in heater incubator. When slide of its cross-linked molecular chains is restricted, energy is able to freeze in its temporary state. It transforms into a permanent state when stored energy is released with its molecular chains sliding under the internal or external stimulus. Furthermore, its structure does not show noticeable change after the deformation-recovery cycle, as illustrated in Fig. 4d. These features enable PVA-based 4D aerogel to exhibit excellent water-induced and thermal-induced shape memory performance.

Supplementary data related to this article can be found at <https://doi.org/10.1016/j.compscitech.2021.108677>.

#### 2.4. A demonstration of potential application

And in fact, the performances of the 4D aerogel are principally determined by the programmable multiscale structure and functional groups. The abundant hydroxyl group of PVA matrix and favorable uranium affinity of the amidoxime group make it possible to construct the functionalized 4D aerogel for radioactive wastes recovery by the precrosslinked ice template technique (Fig. 1). The functionalized PVA-

based 4D aerogel is constructed successfully, as confirmed by Fig. 5 and Fig. S12. It is designated as AO/5-GA-PVA. Of importance, the AO/5-GA-PVA also exhibits a high permeable 3D multiscale spongy framework that is similar to 5-GA-PVA on the microscopic scale, as illustrated in Figs. 5c and 2. Nevertheless, its thermal stability and  $T_g$  decreases after functionalization (Fig. S13). It's very gratifying to see that AO/5-GA-PVA also has excellent stimuli-responsive capacities, which mainly originate from its cross-linked skeleton of the PVA-based 4D aerogel matrix (Table S4). The AO/5-GA-PVA recovered completely permanent state at about 11 s in the water at room temperature (Fig. S14). But the heat transfer ability and stimuli-responsive speed of deployable AO/5-GA-PVA decrease compared with 5-GA-PVA (Fig. S15). Generally, the mass transfer processes of the traditional aerogels are always limited by its volume and the diffusion rate on the vertical direction. In

comparison, the AO/5-GA-PVA with a high permeable multiscale structure also has super hydrophilicity that has been demonstrated by ultrafast permeation in its contact angle tests (Fig. 5d). In particular, the suction resulting from shape memory behavior of this novel 4D aerogel brings substantial advantage in increasing the mass transfer flux. Furthermore, the swelling behavior of AO/5-GA-PVA is another critical influence factor of its stimuli-responsive behavior and beneficial for fast adsorption (Fig. S16).

Fig. 5e and Fig. S17 exhibits the homemade flow-through adsorption performance test system for the pulsion-suction cycle adsorption experiment. The scaffold structure of the acrylic tube gives the sample enough space to recover completely. The preprogrammed AO/5-GA-PVA recovered permanent state at about 5 min in the adsorption experiment (Fig. S18). In solution, a high permeable 3D multiscale

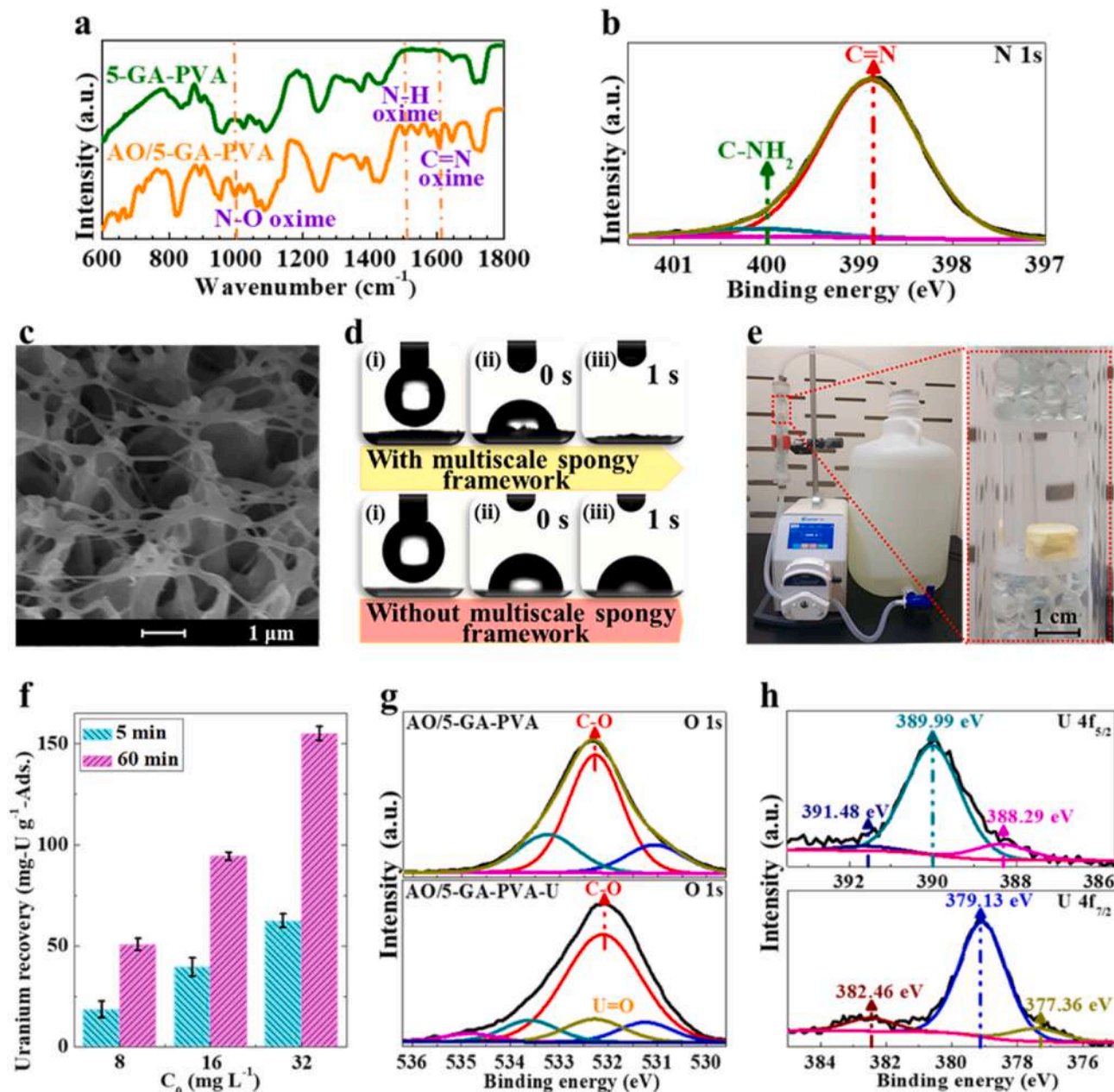


Fig. 5. A demonstration of potential application. (a) FTIR spectra of AO/5-GA-PVA and 5-GA-PVA. (b) High-resolution XPS spectra of the N 1s region for AO/5-GA-PVA. (c) SEM image of AO/5-GA-PVA. (d) The contact angle test of AO/5-GA-PVA with (top) and without (under) multiscale spongy framework at 0s and 1s after touching with water drop, respectively. (e) The representative adsorption experimental setup and a close-up photo of AO/5-GA-PVA before adsorption. (f) The uranium adsorption performance of AO/5-GA-PVA in 20 L 8 mg L<sup>-1</sup>, 16 mg L<sup>-1</sup>, and 32 mg L<sup>-1</sup> uranium solution at 5 min and 60 min. (g, h) High-resolution XPS spectra of: (g) O 1s of AO/5-GA-PVA and uranium loaded AO/5-GA-PVA (AO/5-GA-PVA-U), (h) U 4f of AO/5-GA-PVA-U.

spongy framework, hydrophilic PVA matrix, and suction resulting from its stimuli-responsive behavior will facilitate molecules and ions diffusion to the inner active sites of the spongy framework and even between polymer chains. Therefore, the uranium adsorption quantity of preprogrammed AO/5-GA-PVA has already been able to promptly reach about 60 mg-U/g-Adsorbents in the first 5 min (Fig. 5f). It is faster than other previously reported systems [39]. During the pulsion-suction cycle adsorption experiment, AO/5-GA-PVA revealed good uranium enrichment ability (Movie S5). Its uranium adsorption capacity can reach about 155 mg-U/g-Adsorbents within 60 min. The close-up photos are AO/5-GA-PVA before and after the adsorption experiment (Fig. S17b). There are remarkable distinctions in high-resolution XPS spectra of AO/5-GA-PVA and uranium loaded AO/5-GA-PVA (AO/5-GA-PVA-U) (Fig. 5 and Fig. S19). The binding energy regions around 389.99 eV and 379.13 eV are the  $U 4f_{5/2}$  and  $U 4f_{7/2}$  of AO/5-GA-PVA-U, respectively [39]. From the foregoing, the interaction of uranyl and AO/5-GA-PVA is one of the main influences in uranium recovery. Expectedly, this self-adaptivity 4D aerogel absorbent material has ultrafast adsorption speed, favorable process-ability, low cost, and environmentally friendly. Those are critical for the reduction of time cost and raw material cost in applications. It is expected to provide a universal, simple, and economical preprogrammed fixable and stimuli-responsive strategy for fast enrichment.

Supplementary data related to this article can be found at <https://doi.org/10.1016/j.compscitech.2021.108677>.

All above results suggest that the 4D aerogel and traditional aerogel have conspicuous dissimilarity. As can be seen in Table S3, the 4D aerogel has distinct advantages comparing with traditional aerogel. The 4D aerogel can fix temporary shape and recover original shape under various stimulus without any complicated equipment in the flexible programmable manner, which is unavailable for traditional aerogel. The strength of 4D aerogel is enhanced about 1–2 orders of magnitude compared with traditional aerogel. The 4D aerogel has good thermal stability and hydrophilicity. In Fig. S9 and Fig. S10, its contact angle is about  $0^\circ$  and the swelling degree is above 900 wt %. It has good structural stability in both air and water, while traditional aerogel is fragile or hydrophobic. The structural stability of the 4D aerogel is better than the traditional aerogel. The porous structure, functionalities, and performances of the 4D aerogel can be easily customized by designs of material composition and process parameters to meet various practical applying requirements. These distinctive properties of the 4D aerogel open a new potential field to design and program intelligent structure and system for application in water purification, sensors, super capacitor, biomedicine, oil remediation, and aerospace. And more notably, this new concept and strategy can be popularized to other porous materials bringing above significant advantages and displaying functional properties that are dependent on material and structure.

### 3. Conclusions

In this study, an original 4D aerogel is successfully prepared via precrosslinked and preprogrammed strategy. The 4D aerogel has the capacity of fixable temporary state, programmable temporal-spatial multiscale structure and multi-stimuli responsive performance which are the distinct advantages contrasted with traditional aerogels. The water-induced stimuli-responsive velocity of the 4D aerogel is increased by 2–3 orders of magnitude, especially compared with the most previous water-induced shape memory polymers without 3D structure. In contrast to traditional aerogels, the suction resulting from stimuli-responsive behavior of this 4D aerogel brings substantial advantage in increasing the mass transfer flux. The 4D aerogel provides an attractive system to significantly enhance mass transfer flux and environment-responsive activity of solids. The adsorption of the preprogrammed functionalized 4D aerogel has also been demonstrated. Its high permeable structure, super-hydrophilicity, abundant active functional groups, and suction resulting from its stimuli-responsive behavior facilitate the

interaction between target and its active sites. Moreover, the 4D aerogel also exhibits good thermal-induced shape memory performance, which is obviously different from conventional aerogels. As expected, the customized 4D aerogel can be achieved by optimization of the multi-scale structure, matrix, and functional groups. Its good processibility, multifunctionality, and diversity of its synthetic route are important advantages in practical applications. Interestingly, this concept and approach can be potentially extrapolated to other porous materials with cost-effective and eco-friendly procedures. Overall, these interesting findings will attract much attention in the community of chemists, physicists, and engineers working on porous materials.

### Declaration of competing interest

The authors declare that they have no known competing financial interests or personal relationships that could have appeared to influence the work reported in this paper.

### Acknowledgements

This work was supported by National Natural Science Foundation of China [grant numbers 11902105, 11632005, 11704105]; Hainan Provincial Department of Science and Technology [grant number 2019RC091]; Science Foundation of the National Key Laboratory of Science and Technology on Advanced Composites in Special Environments [grant numbers JCKYS2020603C012]; Hainan University [grant number KYQD(ZR)1813]; and Natural Science Foundation of Shandong Province [grant number ZR2018PEM011].

### Appendix A. Supplementary data

Supplementary data to this article can be found online at <https://doi.org/10.1016/j.compscitech.2021.108677>.

### References

- [1] D.C. Wu, F. Xu, B. Sun, R.W. Fu, H.K. He, K. Matyjaszewski, Design and preparation of porous polymers, *Chem. Rev.* 112 (7) (2012) 3959–4015.
- [2] S.S. Kistler, Coherent expanded aerogels and jellies, *Nature* 127 (1931) 741.
- [3] C.W. Li, L. Qiu, B.Q. Zhang, D. Li, C.Y. Liu, Robust vacuum-/air-dried graphene aerogels and fast recoverable shape-memory hybrid foams, *Adv. Mater.* 28 (7) (2016) 1510–1516.
- [4] G.Y. Li, D.P. Dong, G. Hong, L.F. Yan, X.T. Zhang, W.H. Song, High-efficiency cryothermocells assembled with anisotropic holey graphene aerogel electrodes and a eutectic redox electrolyte, *Adv. Mater.* 31 (25) (2019) 1901403.
- [5] D. Li, Y.H. Wang, F. Long, G. Lin, J. Huang, Solvation-controlled elastification and shape-recovery of cellulose nanocrystal-based aerogels, *ACS Appl. Mater. Interfaces* 12 (1) (2020) 1549–1557.
- [6] F. Guo, X.W. Zheng, C.Y. Liang, Z. Xu, Z.D. Jiao, Y.J. Liu, H.Y. Sun, L. Ma, W. W. Gao, A. Greiner, S. Agarwal, C. Gao, Millisecond response of shape memory polymer nanocomposite aerogel powered by stretchable graphene framework, *ACS Nano* 13 (5) (2019) 5549–5558.
- [7] F. Rechberger, M. Niederberger, Translucent nanoparticle-based aerogel monoliths as 3-dimensional photocatalysts for the selective photoreduction of  $CO_2$  to methanol in a continuous flow reactor, *Mater. Horiz.* 4 (6) (2017) 1115–1121.
- [8] J.J. Mao, J. Iocozzia, J.Y. Huang, K. Meng, Y.K. Lai, Z.Q. Lin, Graphene aerogels for efficient energy storage and conversion, *Energy Environ. Sci.* 11 (4) (2018) 772–799.
- [9] S.Y. Zhao, W.J. Malfait, N.G. Albuquerque, M.M. Koebel, G. Nyström, Biopolymer aerogels and foams: chemistry, properties and applications, *Angew. Chem. Int. Ed.* 57 (26) (2018) 7580–7608.
- [10] L.Z. Guan, M.C. Gutiérrez, M.J. Roldán-Ruiz, R. Jiménez, M.L. Ferrer, F. del Monte, Highly efficient and recyclable carbon-nanofiber-based aerogels for ionic liquid-water separation and ionic liquid dehydration in flow-through conditions, *Adv. Mater.* 31 (39) (2019) 1903418.
- [11] S.C. Han, K. Kang, Another stretching-dominated micro-architected material, *shellular*, *Mater. Today Off.* 31 (2019) 31–38.
- [12] Y. Xie, Y. Meng, W.X. Wang, E. Zhang, J.S. Leng, Q.B. Pei, Bistable and reconfigurable photonic crystals-electroactive shape memory polymer nanocomposite for ink-free rewritable paper, *Adv. Funct. Mater.* 28 (34) (2018) 1802430.
- [13] X.H. Cui, J.W. Chen, Y.T. Zhu, W. Jiang, Natural sunlight-actuated shape memory materials with reversible shape change and self-healing abilities based on carbon nanotubes filled conductive polymer composites, *Chem. Eng. J.* 382 (2020) 122823.

- [14] X. Zhang, C.Y. Zhu, B. Xu, L. Qin, J. Wei, Y.L. Yu, Rapid, localized, and athermal shape memory performance triggered by photoswitchable glass transition temperature, *ACS Appl. Mater. Interfaces* 11 (49) (2019) 46212–46218.
- [15] W.X. Wang, Y.J. Liu, J.S. Leng, Recent developments in shape memory polymer nanocomposites: actuation methods and mechanisms, *Coord. Chem. Rev.* 320–321 (2016) 38–52.
- [16] J.R. Capadona, K. Shanmuganathan, D.J. Tyler, S.J. Rowan, C. Weder, Stimuli-responsive polymer nanocomposites inspired by the sea cucumber dermis, *Science* 319 (5868) (2008) 1370–1734.
- [17] J.S. Leng, X. Lan, Y.J. Liu, S.Y. Du, Shape-memory polymers and their composites: stimulus methods and applications, *Prog. Mater. Sci.* 56 (7) (2011) 1077–1135.
- [18] H. Gao, J.R. Li, F.H. Zhang, Y.J. Liu, J.S. Leng, The research status and challenges of shape memory polymer-based flexible electronics, *Mater. Horiz.* 6 (5) (2019) 931–944.
- [19] T. Sider, Four-dimensionalism (Persistence through time, doctrine of temporal parts, perdurance), *Phil. Rev.* 106 (1997) 197–231.
- [20] D. Lewis, *On the Plurality of Worlds*, Blackwell, Oxford, United Kingdom, 1986.
- [21] N.F. Hardy, V. Goudar, J.L. Romero-Sosa, D.V. Buonomano, A model of temporal scaling correctly predicts that motor timing improves with speed, *Nat. Commun.* 9 (2018) 4732.
- [22] A. Li, S.P. Cornelius, Y.Y. Liu, L. Wang, A.L. Barabási, The fundamental advantages of temporal networks, *Science* 358 (6366) (2017) 1042–1046.
- [23] A. Khaldi, C. Plesse, F. Vidal, S.K. Smoukov, Smarter actuator design with complementary and synergetic functions, *Adv. Mater.* 27 (30) (2015) 4418–4422.
- [24] S. Tibbitts, TED Conferences the Emergence of “4D Printing”, vol. 2, California USA, Long Beach, 2013 presented at.
- [25] C. Lin, J.X. Lv, Y.S. Li, F.H. Zhang, J.R. Li, Y.J. Liu, L.W. Liu, J.S. Leng, 4D-printed biodegradable and remotely controllable shape memory occlusion devices, *Adv. Funct. Mater.* 29 (51) (2019) 1906569.
- [26] H.Q. Wei, Q.W. Zhang, Y.T. Yao, L.W. Liu, Y.J. Liu, J.S. Leng, Direct-write fabrication of 4D active shape-changing structures based on a shape memory polymer and its nanocomposite, *ACS Appl. Mater. Interfaces* 9 (1) (2017) 876–883.
- [27] X. Kuang, D.J. Roach, J.T. Wu, C.M. Hamel, Z. Ding, T.J. Wang, M.L. Dunn, H.J. Qi, Advances in 4D printing: materials and applications, *Adv. Funct. Mater.* 29 (2) (2019) 1805290.
- [28] M.C. Zhang, Y.L. Wang, M.Q. Jian, C.Y. Wang, X.P. Liang, J.L. Niu, Y.Y. Zhang, Spontaneous alignment of graphene oxide in hydrogel during 3D printing for multistimuli-responsive actuation, *Adv. Sci.* 7 (6) (2020) 1903048.
- [29] B. Zhang, K. Kowsari, A. Serjouei, M.L. Dunn, Q. Ge, Reprocessable thermosets for sustainable three-dimensional printing, *Nat. Commun.* 9 (2018) 1831.
- [30] D.K. Patel, A.H. Sakhaei, M. Layani, B. Zhang, Q. Ge, S. Magdassi, Highly stretchable and UV curable elastomers for digital light processing based 3D printing, *Adv. Mater.* 29 (15) (2017) 1606000.
- [31] S.D. Miao, N. Castro, M. Nowicki, L. Xia, H.T. Cui, X. Zhou, W. Zhu, S.J. Lee, K. Sarkar, G. Vozzi, Y. Tabata, J. Fisher, L.G. Zhang, 4D printing of polymeric materials for tissue and organ regeneration, *Mater. Today Off.* 20 (10) (2017) 577–591.
- [32] W.X. Wang, H.B. Lu, Y.J. Liu, J.S. Leng, Sodium dodecyl sulfate/epoxy composite: waterinduced shape memory effect and its mechanism, *J. Mater. Chem.* 2 (15) (2014) 5441–5449.
- [33] M.M. Ma, L. Guo, D.G. Anderson, R. Langer, Bio-inspired polymer composite actuator and generator driven by water gradients, *Science* 339 (6116) (2013) 186–189.
- [34] Y.L. Shao, J. Zhao, Y. Fan, Z.P. Wan, L.S. Lu, Z.H. Zhang, W.H. Ming, L.Q. Ren, Shape memory superhydrophobic surface with switchable transition between “lotus effect” to “rose petal effect”, *Chem. Eng. J.* 382 (2020) 122989.
- [35] D. Chen, X.H. Xia, T.W. Wong, H. Bai, M. Behl, Q. Zhao, A. Lendlein, T. Xie, Omnidirectional shape memory effect via lyophilization of PEG hydrogels, *Macromol. Rapid Commun.* 38 (7) (2017) 1600746.
- [36] W.X. Wang, X.B. Liu, W. Xu, H.Q. Wei, Y.J. Liu, Y. Han, P. Jin, H.J. Du, J.S. Leng, Light-induced microfluidic chip based on shape memory gold nanoparticles/poly (vinyl alcohol) nanocomposites, *Smart Mater. Struct.* 27 (2018) 105047.
- [37] Z. Wang, C. Hansen, Q. Ge, S.H. Maruf, D.U. Ahn, H.J. Qi, Y.F. Ding, Programmable, pattern-memorizing polymer surface, *Adv. Mater.* 23 (32) (2011) 3669–3673.
- [38] X.D. Qi, X.L. Yao, S. Deng, T.N. Zhou, Q. Fu, Water-induced shape memory effect of graphene oxide reinforced polyvinyl alcohol nanocomposites, *J. Mater. Chem.* 2 (7) (2014) 2240–2249.
- [39] D. Wang, J.A. Song, J. Wen, Y.H. Yuan, Z.L. Liu, S. Lin, H.Y. Wang, H.L. Wang, S. L. Zhao, X.M. Zhao, M.H. Fang, M. Lei, B. Li, N. Wang, X.L. Wang, H. Wu, Significantly enhanced uranium extraction from seawater with mass produced fully amidoximated nanofiber adsorbent, *Adv. Energy Mater.* 8 (33) (2018) 1802607.